International Journal of Academic Engineering Research (IJAER)
ISSN: 2643-9085
Vol. 7 Issue 9, September - 2023, Pages: 73-79

Design of 6-Dof Teleoperation-Based Surgical Robot Manipulator Controller

Gitfirul Aziz Widiyanto[1], Sumardi.

Department of Electrical Engineering, Universitas Diponegoro, Semarang, Indonesia
[1] *E-mail: gitfirul.aw@gmail.com*

Abstract: *Minimally Invasive Surgery (MIS) is a surgical method that allows surgeons to access body cavities through a single small incision in the patient's body. MIS has many advantages but requires skill and experience. The development of robotic technology allows surgeons to perform MIS with robot assistance and has been implemented in the medical world. This robot uses a teleoperation principle with a master-slave configuration. One of the problems that occurs in the robot's control with teleoperation, especially in the robot with high degrees of freedom, is the formulation of a mathematical equation from the base to the end effector and the calculation of position and orientation. This paper uses modified DH parameters to simplify robot kinematics and uses forward kinematics calculations with a homogeneous transformation matrix to obtain the position and orientation of the end effector. An exponential moving average filter with α=0.25 was also implemented to reduce the noise. From the forward kinematics test, MAE in the XY field test has a value of 1.789 mm for the X axis and 2.326 mm for the Y axis, and MAE in the XZ field test has 1.743 mm value for the X axis and 1.467 mm for the Z axis.*

Keywords*: forward kinematics, homogeneous transformation matrix, Minimally Invasive Surgery, medical robot*

1. Preface

Minimally Invasive Surgery (MIS) is a surgical method that allows surgeons to access body cavities through a single small incision in the patient's body [1]. This method has become the first choice in surgery because of its advantages [2]. Medical robot technology has developed rapidly, especially in the medical equipment industry [3]. This medical robot can help the doctor perform MIS based on a teleoperation system that consists of a master device and a slave device. However, the cost of procuring and training this medical robot is not cheap. An example of a medical robot that has been used in the medical world is a da Vinci by Intuitive Surgical. This robot has a procurement cost of about $1,200,000 to $1,500,000. Therefore, much research conducted to develop new technology for medical robots for learning purposes.

One of the main problems in manipulator robot control with a teleoperation system is the formulation of mathematical equations for the base position, joint angle, and position of the end effector [4]. This problem can be simplified by using DH parameters and can be solved by using forward kinematics. Another problem in manipulator robot control is the design of the manipulator robot and the control strategy. This is caused by many manipulator robots having application-specific mechanical structures. This problem depends on the design of the desired mechanical structures. Each mechanical design has a different approach to inverse kinematics calculation and has a different control strategy used.

This research will discuss about the design of a 6-DOF teleoperation-based surgical robot manipulator controller as a master device to control the emulator of a 6-DOF surgical robot as a slave device. This surgical robot emulator will be used for learning purposes as an alternative to real surgical robots in robotic surgery training. This master device is designed with STM32 microcontroller and equipped with a filtering process to reduce signal noise.

2. Method

2.1. Robot Kinematics

Kinematics is the branch of mechanical science that learns the movement of an object without considering the mass and force that acting on it [5]. The arm robot has a fixed series of links and joints. Each joint has one degree of freedom that can be translational (prismatic joint) or rotational (revolute joint). This link and joint configuration of the frame-i manipulator controller are shown in Modified DH parameters in Table 1.

Table 1. Modified DH Parameter of Manipulator Controller

i	α_{i-1} (°)	a_{i-1} (mm)	d_i (mm)	θ_i (°)	Joint Type
1	0	0	85	θ_1^*	revolute
2	90	0	0	θ_2^*	revolute
3	0	150	0	θ_3^*	revolute
4	−90	0	150	θ_4^*	revolute
5	90	0	0	θ_5^*	revolute
6	−90	0	0	θ_6^*	revolute

The kinematics diagram of the manipulator controller can be seen in Figure 1.

International Journal of Academic Engineering Research (IJAER)
ISSN: 2643-9085
Vol. 7 Issue 9, September - 2023, Pages: 73-79

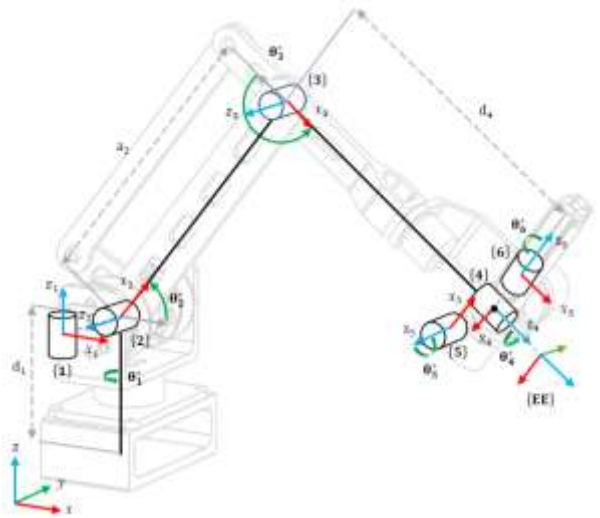

Figure 1. Kinematics Diagram of Manipulator Controller

This manipulator controller consists of 6 revolute joints so that it has 6-DOF. The joint movement changes the relative position of the link connected to that joint. The first three joints are used to adjust the position of the end effector, and the last three joints are used to adjust the orientation of the end effector.

2.2. Forward Kinematics

Forward kinematics is a coordinate mapping of the joint to the end effector pose [5]. This pose of the robot end effector can be obtained by decomposing the homogeneous transformation matrix into a rotation matrix and a translation matrix. The transformation matrix can be obtained from the DH parameter using Equation (1).

$$ {}^{j-1}A_j = \begin{bmatrix} \cos\theta_j & -\sin\theta_j & 0 & a_{j-1} \\ \sin\theta_j \cos\alpha_{j-1} & \cos\theta_j \cos\alpha_{j-1} & -\sin\alpha_{j-1} & -d_j \sin \\ \sin\theta_j \sin\alpha_{j-1} & \cos\theta_j \sin\alpha_{j-1} & \cos\alpha_{j-1} & d_j \cos(\\ 0 & 0 & 0 & 1 \end{bmatrix} \quad (1) $$

Homogeneous transformation matrix obtained by calculating transformation matrix over all frame from the base to the end effector. Because the manipulator controller consists of 6 joint, the form of a homogeneous transformation matrix follow Equation (2).

$$ A_6^0 = A_1^0 A_2^1 A_3^2 A_4^3 A_5^4 A_6^5 \quad (2) $$

The homogeneous transformation matrix in Equation (2) has a general form as Equation (3). This homogeneous transformation matrix is a 4×4 matrix that contains information about rotation and translation from the first frame to the last frame.

$$ A = \begin{bmatrix} A_{11} & A_{12} & A_{13} & A_{14} \\ A_{21} & A_{22} & A_{23} & A_{24} \\ A_{31} & A_{32} & A_{33} & A_{34} \\ 0 & 0 & 0 & 1 \end{bmatrix} \quad (3) $$

Then the translation matrix and the rotation matrix can be decomposed from Equation (3), where the translation matrix is shown in Equation (4) and the rotation matrix is shown in Equation (5).

$$ T = \begin{bmatrix} A_{14} \\ A_{24} \\ A_{34} \end{bmatrix} \quad (4) $$

$$ R = \begin{bmatrix} A_{11} & A_{12} & A_{13} \\ A_{21} & A_{22} & A_{23} \\ A_{31} & A_{32} & A_{33} \end{bmatrix} \quad (5) $$

The translation matrix of Equation (4) represents the position of the end effector relative to the base frame in cartesian coordinate, while the orientation can be obtained from the rotation matrix of Equation (5) by the formula of Equation (6) to the Equation (8) for the Euler representation.

$$ \theta_y = -\sin^{-1}(A_{31}) \quad (6) $$

$$ \theta_x = \tan^{-1}\left(\frac{A_{32}}{A_{33}}\right) \quad (7) $$

$$ \theta_z = \tan^{-1}\left(\frac{A_{21}}{A_{11}}\right) \quad (8) $$

θ_x, θ_y, and θ_z are roll, pitch, and yaw respectively that represent orientation in Euler.

2.3. Exponential Moving Average Filter

Filter is often used to eliminate some frequency to reduce noise that occurs in the signal [6]. Sensor reading signal has the potential to receive a disturbance, either due to the sensor reading itself or operator handling, such as vibration or unintentional hand movement.

Filter used in this design is exponential moving average (EMA) filter. EMA filter is a digital low-pass filter that is more responsive to new data than simple moving average (SMA) [7]. EMA filter has the same noise reduction characteristics as SMA. EMA filter can be formulated by Equation (9).

$$ y_k = \alpha x_k + (1-\alpha) y_{k-1} \quad (9) $$

y_k is the result of EMA calculation at the k-th sampling, y_{k-1} is the result of EMA calculation at the $(k-1)$-th, x_k is the input value at the k-th sampling, and α is the filter coefficient.

3. Result and Discussion

3.1. Sensor Reading Test

3.1.1. Angle Sensor Reading

International Journal of Academic Engineering Research (IJAER)

ISSN: 2643-9085

Vol. 7 Issue 9, September - 2023, Pages: 73-79

Joint angle reading uses three magnetic encoders AS5600 and three hall angle sensors P3022. AS5600 is used to read angle data from joint 1 to joint 3, while P3022 is used to read angle data from joint 4 to joint 6. Figure 2 shows the angle sensor reading in the constant angle value.

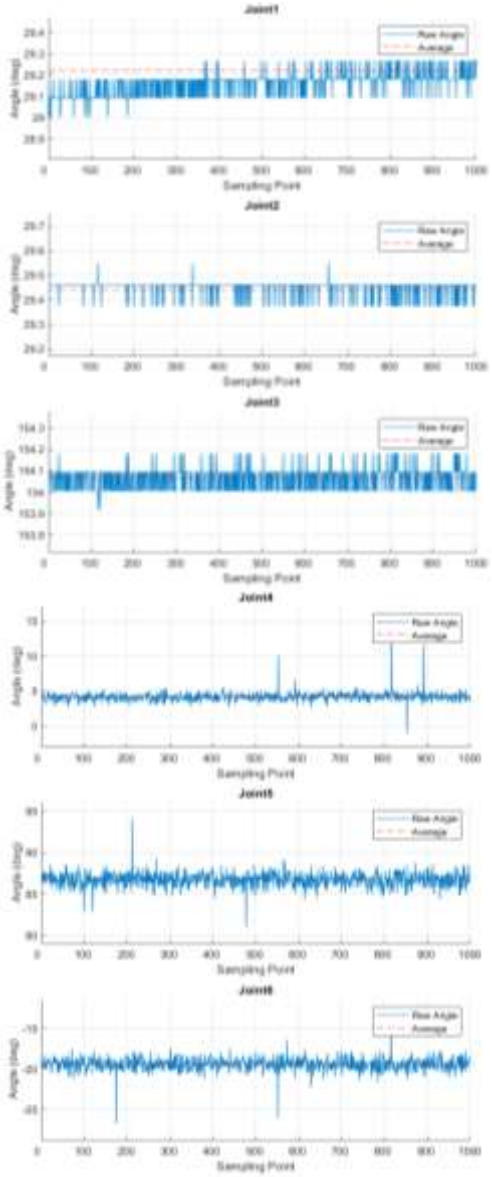

Figure 2. Angle Sensor Reading

From Figure 2, the average value of the sensor reading is assumed to be the right value of the angle. The mean absolute error of the sensor reading is shown in Figure 3. That mean absolute error value represents the noise of the sensor.

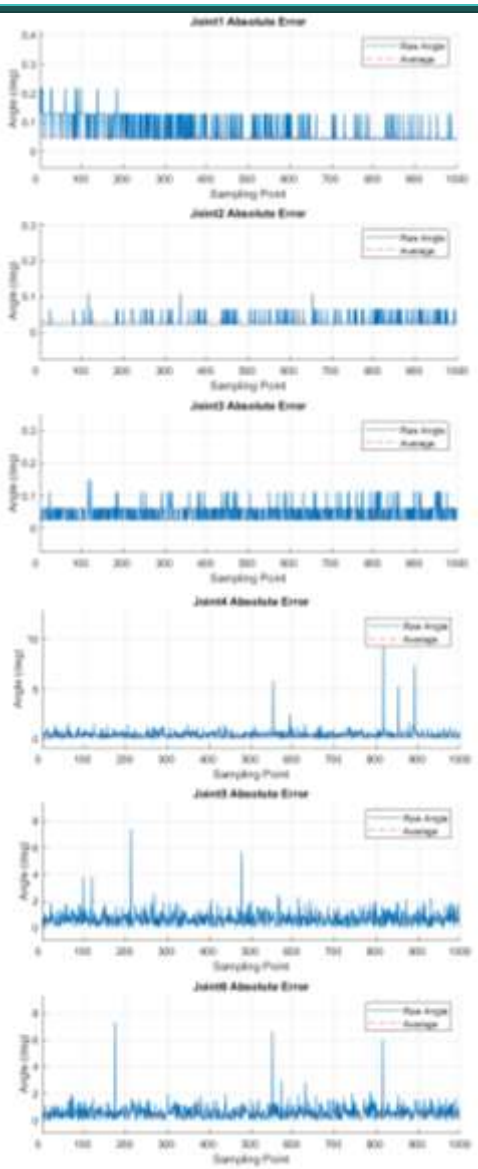

Figure 3. Absolute Error of The Angle Sensor Reading

From Figure 3, AS5600 and P3022 readings have noise. The distribution of noise occurs on the sensors reading shown in Figure 4.

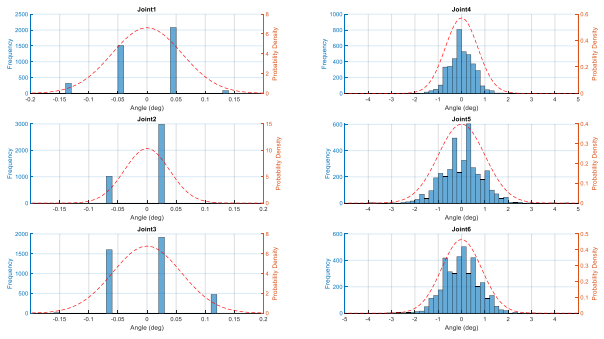

Figure 4. Error Histogram of The Angle Sensor Reading

International Journal of Academic Engineering Research (IJAER)
ISSN: 2643-9085
Vol. 7 Issue 9, September - 2023, Pages: 73-79

From Figure 4, AS5600 sensors have better accuracy compared with P3022 sensors, but P3022 sensors have better precision compared with AS5600 sensors readings.

3.1.2. Filter Implementation

This filter implementation uses $\alpha = 0{,}25$. Figure 5 shows the result of the sensor reading with an EMA filter on the constant angle to test the filter's capability to reduce noise.

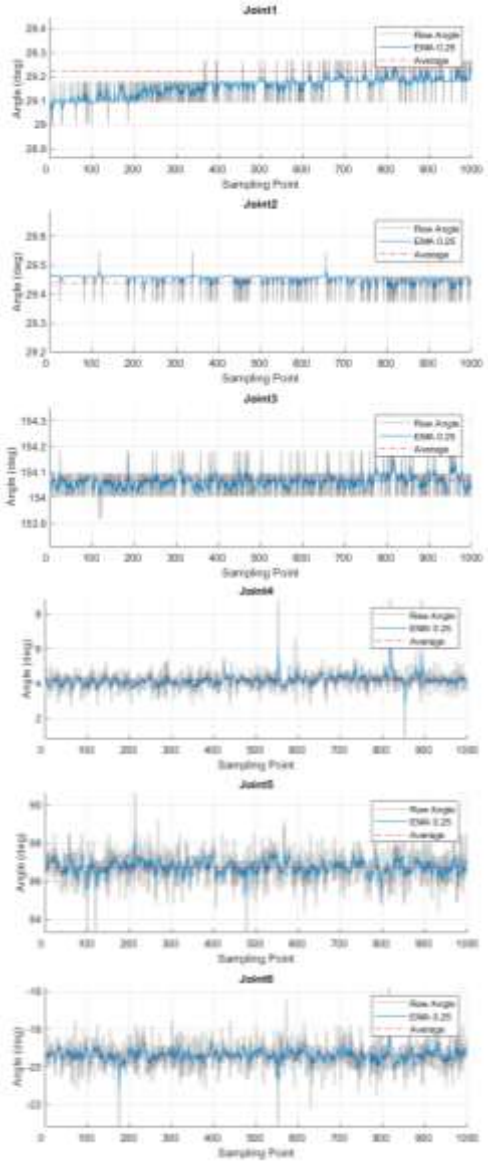

Figure 5. Angle Sensor Reading with EMA Filter

The sensor reading without filter is represented by the gray line while the sensor reading with filter is represented by the blue line. From Figure 5, the EMA filter seems can reduce noise that occurs on the sensor readings. Figure 6 shows the absolute error of the sensor reading with an EMA filter that represents the noise of the sensor readings.

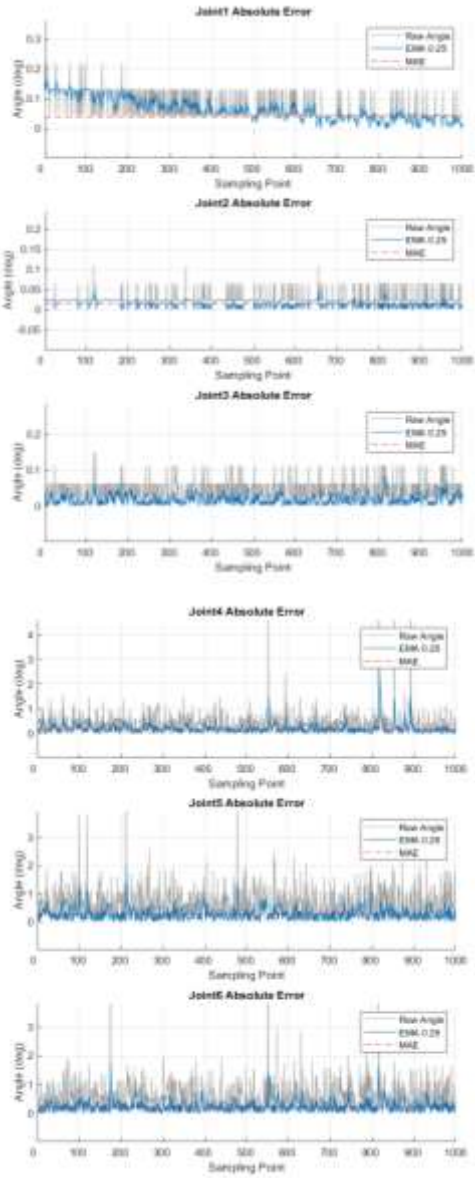

Figure 6. Absolute Error of The Angle Sensor Reading with EMA Filter

Figure 7 shows the noise distribution of sensor reading with an EMA filter.

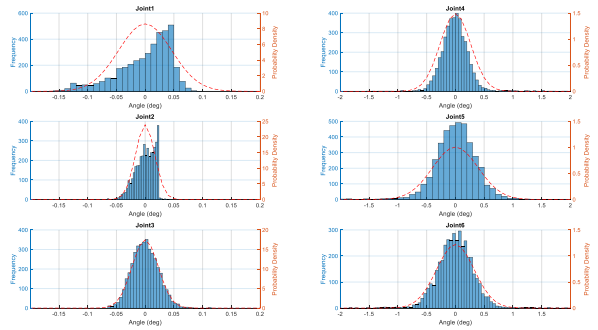

Figure 7. Error Histogram of The Angle Sensor Reading with EMA Filter

From Figure 7, EMA filter implementation can increase the accuracy and precision of the angle sensor AS5600 and P3022. To test filter response toward the new data, a circular movement test was conducted with a path circumference of 463 mm. Figure 8 shows the result of this test.

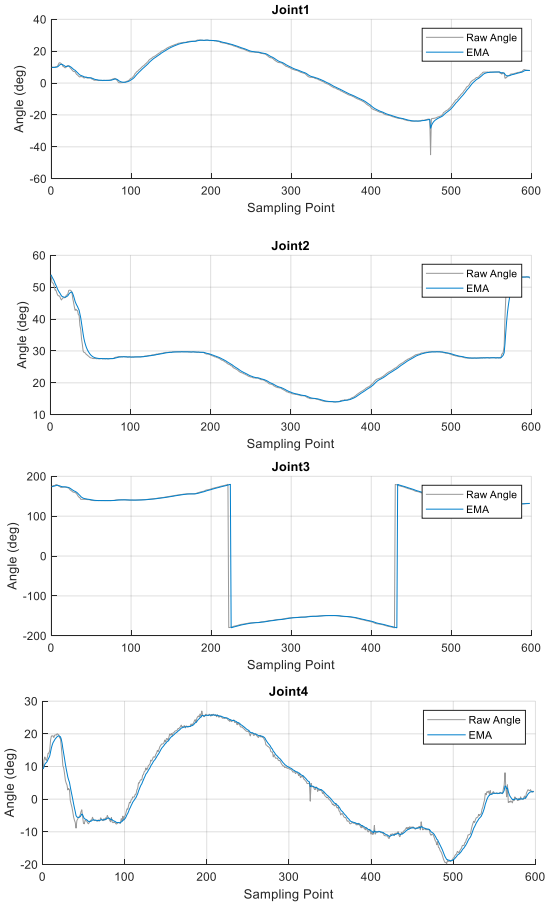

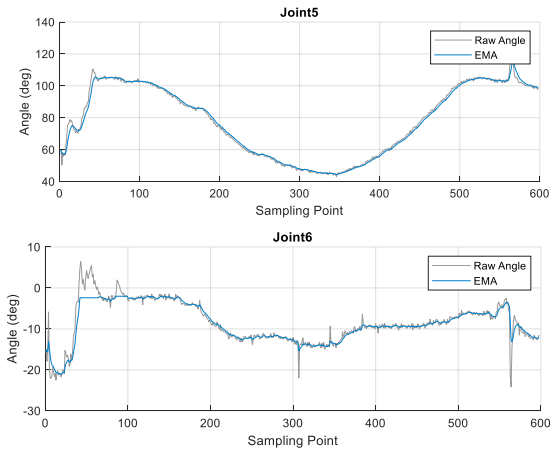

Figure 8. Sensor Reading with EMA Filter on The Circular Path

From Figure 8, the EMA filter can follow the data change over time while reducing the noise.

3.2. Forward Kinematics Test

Forward kinematics test is conducted by moving the end effector of the manipulator controller to follow the test path of Figure 9 over two planes, XY-plane and XZ-plane.

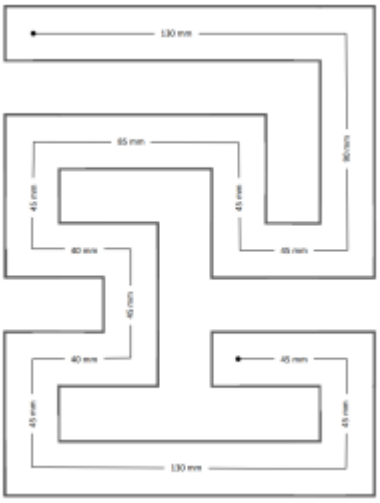

Figure 9. Path of Forward Kinematics Test

This path has a total length of 830 mm, with 515 mm about the X-axis and 315 mm about the Y/Z-axis.

3.2.1. XY-Plane Test

The graphic of the XY-plane position change can be seen in Figure 10. From this test, obtained MAE values of $MAE_X = 1.789$ mm and $MAE_Y = 2.326$ mm, with a total MAE of 3.809 mm.

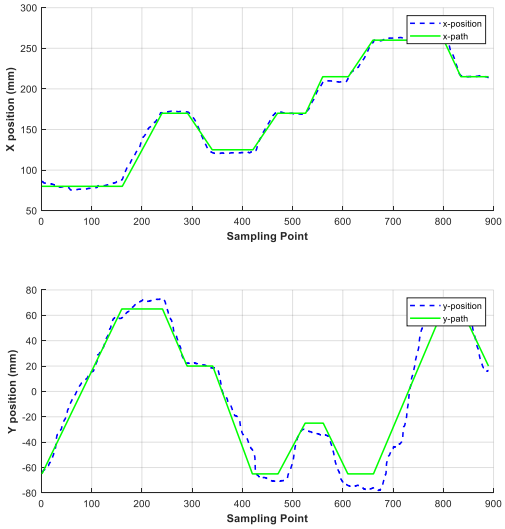

Figure 10. End Effector Position Change of XY-plane Test

The result of the end effector position movement from this test can be seen in Figure 11.

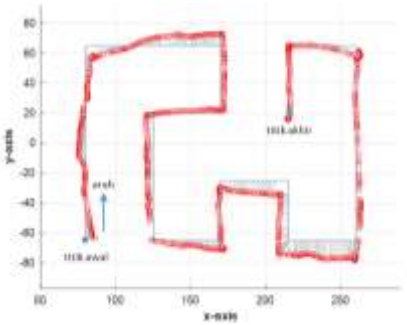

Figure 11. End Effector Position of XY-plane Test

Figure 12 shows the visualization of the forward kinematics test result on the XY-plane.

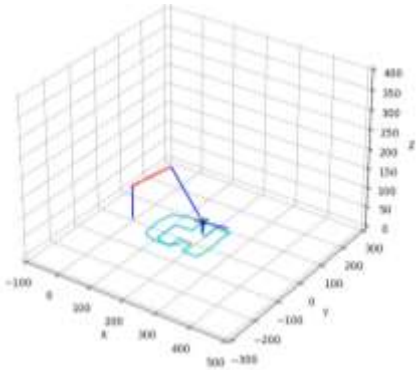

Figure 12. Forward Kinematics Test Result on The XY-Plane

From Figure 12, can be seen that the end effector can follow the test path.

3.2.2. XZ-Plane Test

The graphic of the XZ-plane position change can be seen in Figure 13. From this test, obtained MAE value of $MAE_X = 1.743$ mm and $MAE_Z = 1.467$ mm, with a total MAE of 2.933 mm.

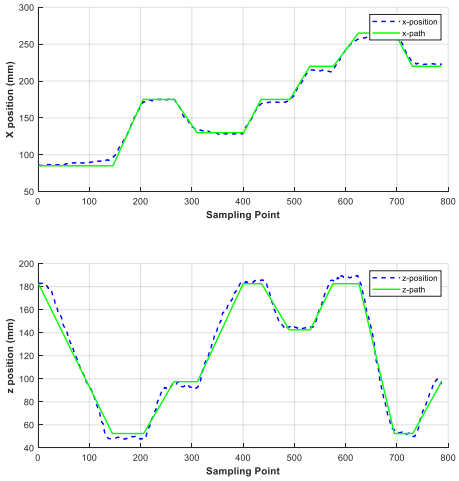

Figure 13. End Effector Position Change of XZ-plane Test

The result of the end effector position movement from this test can be seen in Figure 14.

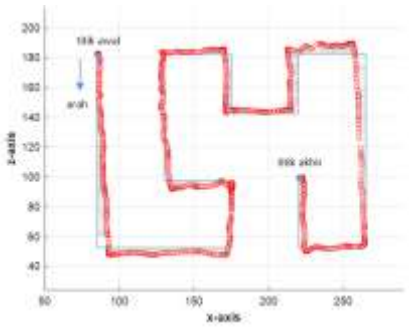

Figure 14. End Effector Position of XZ-plane Test

Figure 15 shows the visualization of the forward kinematics test result on the XZ-plane.

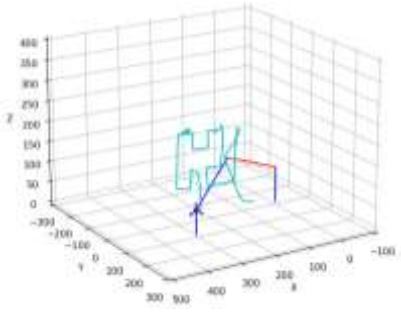

Figure 15. Forward Kinematics Test Result on The XZ-Plane

From Figure 15, can be seen that the end effector can follow the test path.

3.2.3. Result of Forward Kinematics Test

MAE value from the forward kinematics test is shown in Table 2.

Table 2. MAE of Forward Kinematics Test

Axis	MAE_X	MAE_Y	MAE_Z	MAE
XY	1,789 mm	2,326 mm	–	3,809 mm
XZ	1,743 mm	–	1,467 mm	2,933 mm

A comparison of MAE value is shown in Figure 16.

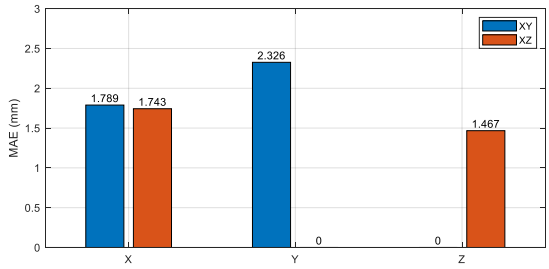

Figure 16. MAE of Forward Kinematics Test

From Table 2 and Figure 16, the XY-plane test has MAE value of $MAE_X = 0.347$ mm and $MAE_Y = 0.738$ mm. XZ-plane test has MAE value of $MAE_X = 0.384$ mm and $MAE_Z = 0.466$ mm.

3.2.4. Free-Space Moving Test

This test is done by moving the manipulator controller over the XY-plane to follow the circular path while maintaining the X-axis orientation frame of the end effector always heads to the circle center. The result of this test can be seen in Figure 17.

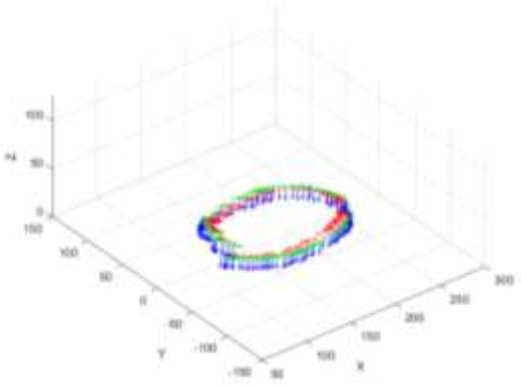

Figure 17. Free-Space Moving Test Result

Figure 17 shows that the X-axis orientation frame of the end effector (red) always heads to the circle center. Y-axis orientation frame of end effector (green) head to direction of movement. Z-axes orientation frame of end effector (blue) head to −Z direction.

4. Conclusion

Forward kinematics calculation with a homogeneous transformation matrix succeeds in giving position and orientation data of the end effector based on joint value. The result of the position test on the XY-plane test has $MAE_X = 1.789$ mm and $MAE_Y = 2.326$ mm, while the XZ-plane test has $MAE_X = 1.743$ mm and $MAE_Z = 1.467$ mm. Free-space moving test results show that the manipulator controller can provide the right orientation data.

References

[1] M. M. Marinho, M. C. Bernardes, and A. P. L. Bo, "Using General-Purpose Serial-Link Manipulators for Laparoscopic Surgery with Moving Remote Center of Motion," *J. Med. Robot. Res.*, vol. 01, no. 04, p. 1650007, Dec. 2016, doi: 10.1142/S2424905X16500070.

[2] T. Morvan, M. Martinsen, M. Reimers, E. Samset, and O. J. Elle, "Collision detection and untangling for surgical robotic manipulators," *Int. J. Med. Robot. Comput. Assist. Surg.*, vol. 5, no. 3, pp. 233–242, Sep. 2009, doi: 10.1002/rcs.247.

[3] G.-Z. Yang *et al.*, "Medical robotics—Regulatory, ethical, and legal considerations for increasing levels of autonomy," *Sci. Robot.*, vol. 2, no. 4, Mar. 2017, doi: 10.1126/scirobotics.aam8638.

[4] I. Agustian, N. Daratha, R. Faurina, A. Suandi, and S. Sulistyaningsih, "Robot Manipulator Control with Inverse Kinematics PD-Pseudoinverse Jacobian and Forward Kinematics Denavit Hartenberg," *J. Elektron. dan Telekomun.*, vol. 21, no. 1, p. 8, 2021, doi: 10.14203/jet.v21.8-18.

[5] P. Corke, *Robotics, Vision and Control*, 2nd ed., vol. 118. Cham: Springer International Publishing, 2017. doi: 10.1007/978-3-319-54413-7.

[6] DEWESoft, "Signal filtering, Signal suppression, Signal processing," 2020. https://training.dewesoft.com/online/course/filters (accessed Jul. 19, 2023).

[7] J. G. Silva, J. O. De Aquino Limaverde Filho, and E. L. Feitosa Fortaleza, "Adaptive Extended Kalman Filter using Exponencial Moving Average," *IFAC-PapersOnLine*, vol. 51, no. 25, pp. 208–211, 2018, doi: 10.1016/j.ifacol.2018.11.106.